Atmos. Chem. Phys., 11, 7755–7765, 2011
www.atmos-chem-phys.net/11/7755/2011/
doi:10.5194/acp-11-7755-2011
© Author(s) 2011. CC Attribution 3.0 License.

Atmospheric Chemistry and Physics

Measurements of gaseous H_2SO_4 by AP-ID-CIMS during CAREBeijing 2008 Campaign

J. Zheng[1], M. Hu[2], R. Zhang[1,2], D. Yue[2,*], Z. Wang[2], S. Guo[2], X. Li[2,5], B. Bohn[5], M. Shao[2], L. He[3], X. Huang[3], A. Wiedensohler[4], and T. Zhu[2]

[1]Department of Atmospheric Sciences, Texas A&M University, College Station, TX 77843-3150, USA
[2]State Key Joint Laboratory of Environmental Simulation and Pollution Control, College of Environmental Sciences and Engineering, Peking University, Beijing 100871, China
[3]Key Laboratory for Urban Habitat Environmental Science and Technology, Shenzhen Graduate School of Peking University, Shenzhen 518055, China
[4]Leibniz Institute for Tropospheric Research, Permoserstrasse 15, Leipzig 04318, Germany
[5]Institute für Energie- und Klimaforschung Troposphäre (IEK-8), Forschungszentrum Jülich, 52425 Jülich, Germany
[*]now at: Guangdong Environmental Monitoring Center, Guangdong, 510308, China

Received: 19 January 2011 – Published in Atmos. Chem. Phys. Discuss.: 10 February 2011
Revised: 20 July 2011 – Accepted: 20 July 2011 – Published: 3 August 2011

Abstract. As part of the 2008 Campaign of Air Quality Research in Beijing and Surrounding Regions (CAREBeijing 2008), measurements of gaseous sulfuric acid (H_2SO_4) have been conducted at an urban site in Beijing, China from 7 July to 25 September 2008 using atmospheric pressure ion drift – chemical ionization mass spectrometry (AP-ID-CIMS). This represents the first gaseous H_2SO_4 measurements in China. Diurnal profile of sulfuric acid is strongly dependent on the actinic flux, reaching a daily maximum around noontime and with an hourly average concentration of 5×10^6 molecules cm^{-3}. Simulation of sulfuric acid on the basis of the measured sulfur dioxide concentration, photolysis rates of ozone and nitrogen dioxide, and aerosol surface areas captures the trend of the measured H_2SO_4 diurnal variation within the uncertainties, indicating that photochemical production and condensation onto preexisting particle surface dominate the observed diurnal H_2SO_4 profile. The frequency of the peak H_2SO_4 concentration exceeding 5×10^6 molecules cm^{-3} increases by 16 % during the period of the summer Olympic Games (8–24 August 2008), because of the implementation of air quality control regulations. Using a multivariate statistical method, the critical nucleus during nucleation events is inferred, containing two H_2SO_4 molecules ($R^2 = 0.85$). The calculated condensation rate of H_2SO_4 can only account for 10–25 % of PM_1 sulfate formation, indicating that either much stronger sulfate production exists at the SO_2 source region or other sulfate production mechanisms are responsible for the sulfate production.

1 Introduction

Gaseous sulfuric acid (GSA) is of critical atmospheric interest for its important role in various atmospheric processes, such as new particle formation (Seinfeld and Pandis, 1998; Finlayson-Pitts and Pitts, 1999), modification of optical properties and hygroscopicity of preexisting aerosols (Khalizov et al., 2009a, b), and formation of polar stratospheric clouds (Zhang et al., 1993a, b, 1996). GSA is predominantly formed through the gas-phase reaction between hydroxyl radical (OH) and sulfur dioxide (SO_2) in the presence of oxygen (O_2) and water (H_2O).

$$SO_2 + OH + M \rightarrow HSO_3 + M \quad \text{(R1)}$$

$$HSO_3 + O_2 \rightarrow SO_3 + HO_2 \quad \text{(R2)}$$

$$SO_3 + H_2O + M \rightarrow H_2SO_4 + M \quad \text{(R3)}$$

GSA forms strong inter-molecular hydrogen bonds with H_2O, and H_2SO_4 has a low saturation vapor pressure at atmospherically relevant relative humidity (Zhang et al., 1993a;

Correspondence to:
M. Hu (minhu@pku.edu.cn)
R. Zhang (zhang@ariel.met.tamu.edu)

Zhao et al., 2009). The fate of GSA in the atmosphere depends on the available surface area of preexisting aerosols. H_2SO_4 also forms molecular complexes with inorganic and organic species (Zhang et al., 2004). The size of these complexes is usually less than a few nanometers, below the detection limit of conventional instrumentation for nanoparticles. New particle formation includes nucleation to form the critical nucleus and subsequent growth of the critical nucleus to a detectable size of nanoparticles (L. Wang et al., 2010; Zhang, 2010). Although the detailed mechanisms of atmospheric aerosol nucleation and growth is still a subject of active research (Kulmala et al., 2004; Arnold, 2006; Nadykto and Yu, 2007; Young et al., 2008; Sipila et al., 2010; Zhang, 2010), H_2SO_4 is commonly considered as one of the dominant components of newly formed nanoparticles.

Atmospheric aerosols have important implications on the solar and terrestrial radiation budget (IPCC, 2007; Zhang et al., 2007) and multi-phase chemical processes (Molina et al., 1997). Freshly emitted soot contains mainly elementary carbon (EC) and to a lesser extent organic matter (OM). EC absorbs solar and terrestrial radiation and is also referred to as black carbon (BC). Fresh soot is largely hydrophobic and does not serve as cloud condensation nuclei (CCN) until a high supersaturation is reached (Zhang et al., 2008). However, after exposure to GSA, soot particles become hydrophilic, because of irreversible uptake of GSA (Zhang and Zhang, 2005). Consequently, aged soot is more prone to wet deposition and has a smaller atmospheric residence time. Internally mixed soot particles with H_2SO_4 (or neutralized by ammonia to form ammonium sulfate) enhance light absorption and scattering, especially at higher mass fraction of sulfate (Cheng et al., 2008; Khalizov et al., 2009a). GSA significantly influences the soot-aging process by modifying the morphology, optical properties, and hygroscopicity of soot particles (Zhang et al., 2008). Measurements of GSA provide a valuable input for evaluation of the soot aging process under atmospheric conditions. Furthermore, sulfuric acid can efficiently catalyze aqueous reactions of organic compounds, formed from photo-oxidation of volatile organic compounds (Suh et al., 2001; Zhang et al., 2002b), contributing to the formation of secondary organic aerosols (Zhao et al., 2005, 2006).

Because of rapid economic development and urbanization, Beijing has become one of the most populated cities in China. Increasing demand for energy in both industrial and domestic sectors leads to large fossil fuel consumption, with annual emissions of 2.39×10^5 tons of nitrogen oxides (NO_x = NO + NO_2), 2.4×10^5 tons of volatile organic compounds (VOCs), 1.9×10^5 tons of sulfur dioxide (SO_2), and 5.8×10^4 tons of soot (Chan and Yao, 2008). Particularly, power plants, domestic heating, and industries respectively account for 49 %, 26 %, and 24 % of the SO_2 emission inventories (Chan and Yao, 2008). Consequently, Beijing is frequently experiencing severe air pollution events, which are characterized by high concentrations of ozone (O_3) and particulate matter (PM) and severe deterioration in visibility. Rapid soot aging has been reported in the Beijing area, when the single scattering albedo of the aerosols increases to values above 0.9 within several hours due to secondary aerosol formation and condensation growth (Cheng et al., 2009).

Because of concerns regarding air quality during the 2008 Olympic Games period, the Beijing Municipal Environmental Protection Bureau (EPB) adopted a series of air quality control measures (Wang et al., 2009). On 20 July, a rule for odd/even numbers of the registration plate of automobiles was applied, aiming a reduction of 50 % of the traffic volume from the private car sector. During the Olympic Games period, an extra 20 % of state owned vehicles were off the road, but extra diesel buses were added to the public transportation fleet to accommodate the increasing demand for transit among different stadiums. In addition, certain factories surrounding the Beijing area were temporarily shut down. After the Paralympics ended on 17 September, most of the regulations were lifted and on-road traffic increased. The Campaign of Air Quality Research in Beijing and Surrounding Regions (CAREBeijing 2008) was one of a series of comprehensive field studies (e.g. CAREBeijing 2006 and 2007) targeting the understanding of the chemical and physical processes responsible for the air pollution episodes. During the CAREBeijing 2008 campaign, a suite of state-of-the-art instruments were deployed to measure trace gases, meteorological parameters, and aerosol number size distribution and chemical composition (PM_1).

This paper reports measurements of GSA during the CAREBeijing 2008 field study. In a separate publication, the role of GSA in new particle formation and growth has been investigated by Yue et al. (2010). Data validation of the GSA measurements is performed using a normalized sequential difference analysis (NSD). Meteorological effects on GSA are also discussed. The GSA diurnal features are presented and the influences from the administrative regulations on GSA measurements are discussed. Moreover, the fate of GSA in the Beijing urban environment is evaluated, focusing on its photochemical production and condensation sink. By applying a multivariate statistical method, the number of H_2SO_4 molecules in the critical nuclei is estimated during nucleation events. The contribution of H_2SO_4 to particulate sulfate is assessed.

2 Experimental

2.1 GSA measurements

The observation site was on the rooftop of a six-story building on the campus of the Peking University (39°59′21″ N and 116° 18′26″ E), located in the NW part of the urban Beijing area. GSA was measured with atmospheric pressure ion-drift chemical ionization mass spectrometry (AP-ID-CIMS). The detailed instrument description has been

provided elsewhere (Fortner et al., 2004; Zheng et al., 2010). Briefly, the AP-ID-CIMS consisted of an inlet (10 cm ID and 60 cm long), an Am-241 ion source, an atmospheric pressure ion-drift tube, and a quadrupole mass spectrometer (QMS). The AP-ID-CIMS was housed inside an air-conditioned observatory. To minimize wall loss, the inlet was machined into a scooped-shape and the sampling rate was kept at about 1200 standard liters per minute (slpm). About 55 slpm of the total air sample was introduced into the drift tube, where ambient H_2SO_4 underwent proton-transfer reactions with nitrate anion ($NO_3^-\cdot HNO_3$) (*m/e* 125), generated from HNO_3 vapor by α particle radiation, to form $HSO_4^-\cdot HNO_3$ (*m/e* 160). All reagent and product ions were sequentially monitored by the QMS in selective ion monitor (SIM) mode for about 12 s. Instrument calibrations were conducted twice a week with a custom-made water photolysis GSA primary source adjustable in the concentration range of 10^7 to 10^8 molecules cm^{-3}. The calibration device was a 0.5-in OD UV point light source, consisting of a mercury lamp (UVP, 90-0012-01), a bandpass filter centered at 185 ± 25 nm (OMEGA Optical, XB32), and a set of turbulence-inducing fins. During calibration, H_2O molecules in the ambient air were photolyzed by the 184.9 nm radiation into OH radicals, which were converted into GSA (shown as Reactions R1–R3) by excess SO_2 (Sigma-Aldrich) supplied in the front of the inlet. The formed GSA concentration was determined by the H_2O concentration and the 184.9 nm radiation intensity. The H_2O concentration was determined by the ambient temperature and relative humidity obtained from the meteorological station measurements. The 184.9 nm radiation intensity was measured by a CsI phototube (Hamamatsu R5764) certified by the National Institute of Standards and Technology (NIST). Since the 184.9 nm radiation attenuated significantly in the air, a set of fins were used to evenly distribute the formed GSA inside the inlet. A series of orifices with diameters ranging from 0 to 5 mm were used to vary the light source intensity and the formed GSA concentration. For a 5 min average time, the detection limit for GSA was about 10^5 molecules cm^{-3}. From in-situ calibrations, the sensitivity of AP-ID-CIMS (counts per second (Hz) per unit H_2SO_4 molecule cm^{-3}) varied within 36 % of the mean value (5×10^4 molecules cm^{-3} per Hz signal) and was reported as the uncertainty in the present work. Since the GSA source was positioned at the front of the inlet, the inlet wall loss was accounted for from the calibration results. The background signal of the AP-ID-CIMS was occasionally checked by covering the drift-tube inlet with a nylon cloth. Due to the high flow rate, only one layer of nylon cloth was used. At nighttime when ambient GSA was low, a background signal of a few counts was treated as the instrument background.

2.2 Aerosol and trace gas measurements

Aerosol number size distribution (3 nm to 10 µm) was measured by a twin differential mobility particle sizer (TDMPS) and an aerodynamic particle sizer (APS) (TSI Inc., model 3321). The TDMPS consists of two Hauke-type differential mobility analyzers (DMA) and two condensation particle counters (CPC, TSI Inc., model 3010 and 3025) and are used to measure the particle size distributions from 3 to 900 nm (Stokes diameter). The APS is used to measure aerosols with aerodynamic diameter between 500 nm and 10 µm. A detailed description and operation conditions of the TDMPS and APS are provided by Yue et al. (2010). The concentration of particle surface area is integrated from the particle number distribution, by assuming a spherical geometry for the particle. Error sources in aerosol surface area measurements include the DMA transfer function, the CPC counting efficiency, the flow rate, and the data inversion process. Considering these error sources, the uncertainty is estimated as 10 % for particles between 25 and 900 nm.

An Aerodyne High-Resolution Time-of-Flight Aerosol Mass Spectrometer (HR-ToF-AMS) was deployed to characterize particle chemical compositions. The detailed instrumental description of HR-ToF-AMS has been given by DeCarlo et al. (2006). The operation procedure of the HR-ToF-AMS during the 2008 CAREBeijing campaign has been described by Huang et al. (2010) in a companion paper of this special issue. Briefly, the HR-ToF-AMS was operated sequentially in a cycle of 5 modes every 10 min, including a 2 min V-mode to obtain the mass concentrations of the non-refractory species, a 2 min W-mode to obtain high resolution mass spectral data, a 4 min separate PToF (particle time-of-flight) mode to determine size distributions of species under the V-mode, and a 2 min Soft-EI mode using a lower EI voltage ($\sim$13 eV).

The photolysis frequencies of O_3 (J_{O^1D}) and NO_2 (J_{NO_2}) were measured by specifically designed filter radiometers provided by Forschungszentrum Jülich, Germany (FZJ). The instruments were calibrated at FZJ with a reference spectroradiometer before and after the campaign. The accuracy of the photolysis frequency measurements was estimated to be 10 % at solar zenith angles smaller than 80° (Bohn et al., 2008).

Measurements of meteorology parameters including wind direction, wind speed, temperature, pressure, relative humidity, precipitation, UVA and UVB were conducted with a LASTEM auto meteorology station (LSI-LASTEM, M7115). SO_2 was measured with a commercial fluorescence sulfur dioxide analyzer (ECOTECH, EC9850). O_3 and NO_2 were both measured with Thermo Scientific instruments (Models 49C and 42C). All trace gas instruments were maintained and calibrated routinely and the measurements were reported with an uncertainty of 1 %.

3 Results and discussion

3.1 Instrument performance and meteorological effect

Accurate measurements of GSA represent a great challenge because of its low concentration and sticky nature. Since the instrument was located about 5 m below the observatory rooftop and the inlet can only be positioned toward the east, these physical conditions may cause some bias for the GSA measurements to represent the real ambient level of GSA, especially under certain wind direction and a high wind speed. In addition, wind can induce turbulence at the inlet, causing wall losses. A normalized sequential difference (NSD) analysis of the GSA data is performed to evaluate the performance of the AP-ID-CIMS instrument and measurement results. NSD at time t is calculated from (Arnold et al., 2007)

$$\mathrm{NSD}_t = \frac{C_t - C_{t-1}}{\sqrt[2]{C_t \times C_{t-1}}} \quad (1)$$

where C_t and C_{t-1} correspond to two consecutive GSA data points at time t and $t-1$, respectively. NSD represents the consistency of the instrument performance. Since all the factors affecting the observation results are random in nature, NSD_t is expected to exhibit a normal distribution with a mean of zero if there is not a systematic bias associated with the instrument. Figure 1a shows the frequency histogram of the NSD plotted in bins of 0.023 width. The histogram appears to be nearly a Gaussian distribution with a slight positive skewness. A p-value of 0.24 (larger than 0.05) is obtained from a standard t-test between the NSD and a randomly generated normal distribution with the same standard deviation as the calculated NSD but a mean value of zero, indicating that the positive skewness is statistically insignificant. Therefore, the GSA data shows no systematic instrument bias in either direction. Similarly, by plotting NSD with GSA concentration (Fig. 1b), it is demonstrated that within the observed GSA concentration range, the NSD is also normally distributed, i.e. the AP-ID-CIMS does not show a systematic bias within the range of observed GSA level.

GSA is highly sticky to almost all kind of surfaces. In order to minimize the inlet losses, a short inlet and a high sampling flow rate are used for the GSA measurement, with a similar working principle as a fast-flow reactor (Seeley et al., 1993). The inlet is a 60 cm long 10 cm ID aluminum tube, allowing about 1200 slpm sample flow. The sample residence time is about 0.2 s. Meanwhile, the fast flow rate induces a high Reynolds number turbulent flow with an eddy scale approaching the diameter of the inlet. Consequently, the small eddies induced by the surface friction are suppressed by the large eddies dominated by the inertial force. GSA molecules at the center of the flow must penetrate the small eddies at the edge before colliding with the inlet surface. Hence, inlet losses are minimized. Our ambient test results show that the instrument signal increases with a higher flow rate with respect to a similar GSA concentration. However, wind gusts

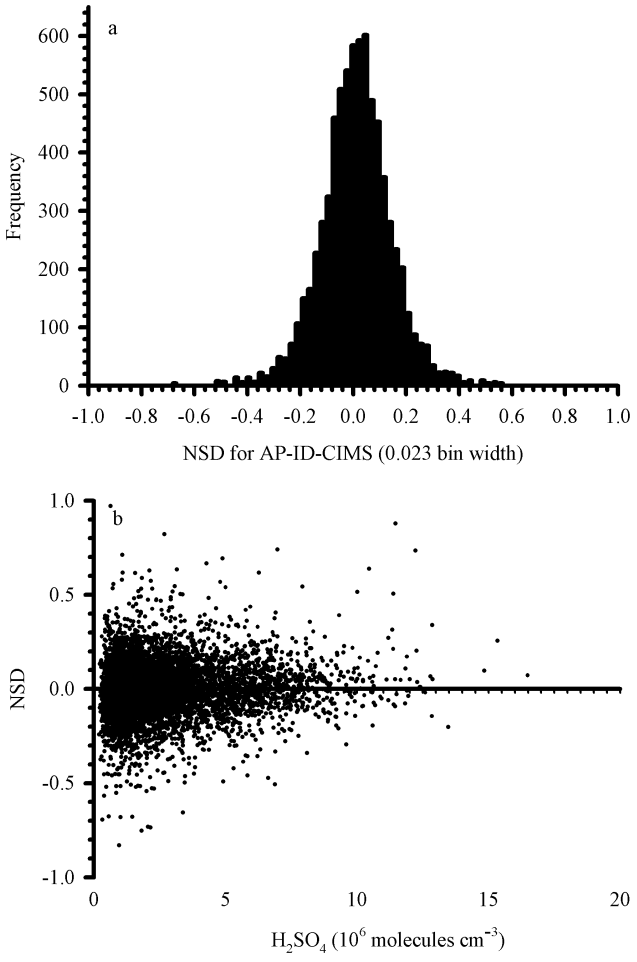

Fig. 1. (a) Frequency histogram of normalized sequential difference (NSD) for the AP-ID-CIMS; **(b)** scatter plot of NSD with GSA concentration.

with a speed of a few m s^{-1} may still impact the inlet flow pattern, especially when the wind direction is perpendicular to the inlet. Figure 2 presents (a) a polar plot of the NSD with wind direction (North = 0 degree) and (b) a scatter plot of NSD with wind speed. Overall, NSD scatters in all wind directions with a slight bias under NW wind, but NSD is symmetrically distributed at any wind speed. This result is explained by the orientation of the inlet, i.e. when wind blows from perpendicular to the inlet or at a higher speed, more wall loss is expected as the air flow changes direction for both cases, but this bias is statistically insignificant.

3.2 H_2SO_4 measurements

The measurement period spans from 7 July to 25 September, covering the entire period of the XXIX Olympic Games and the Paralympics. Because GSA is photochemically produced and readily lost to aerosol surfaces, its concentration is expected to follow solar radiation intensity and is

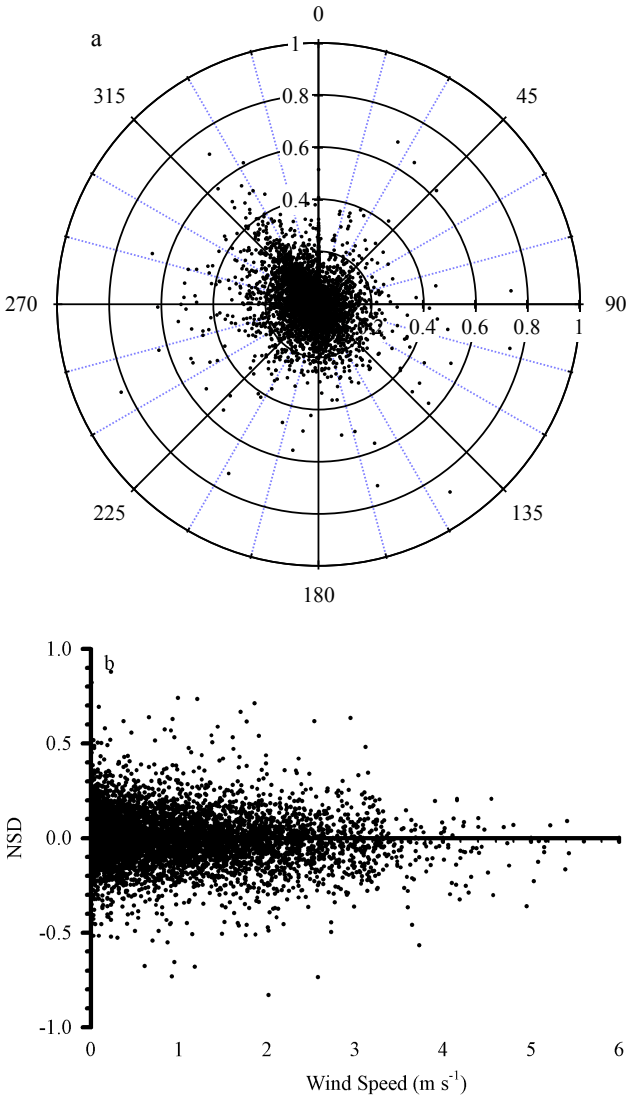

Fig. 2. **(a)** A plot of NSD with wind direction (North represented by 0 degree). **(b)** A scatter plot of NSD with wind speed.

anti-correlated with the aerosol loading. Figure 3 shows the time series of GSA concentration measured during the 2008 CAREBeijing field campaign. The gaps within the series are due to interruption of power supply or instrument calibration. Diurnally, GSA typically remains a minimum value from late night to early morning and reaches a daily peak at noontime. The maximum peak value of GSA is measured on 10 September, with a concentration of 1.9×10^7 molecules cm^{-3}.

The reaction between SO_2 and OH (Reactions R1 to R3) represents the primary pathway to form GSA (Finlayson-Pitts and Pitts, 1999), whereas GSA is readily removed by condensing onto aerosol surfaces. Simultaneous measurements of GSA and aerosol surface area present a unique opportunity to evaluate the competition between production and removal of GSA. The steady-state GSA concentration is calculated from

$$P_{\mathrm{GSA}} = L_{\mathrm{GSA}} \tag{2}$$

where $P_{\mathrm{GSA}} = k_{\mathrm{OH+SO_2}}[\mathrm{OH}][\mathrm{SO_2}]$ and $L_{\mathrm{GSA}} = \frac{\gamma \cdot S \cdot \bar{v}}{4}[\mathrm{H_2SO_4}]$ (Freiberg and Schwartz, 1981), P_{GSA} and L_{GSA} denote GSA production and loss, respectively, $k_{\mathrm{OH+SO_2}}$ is the rate constant of Reaction (R1) calculated according to JPL (2006) with an uncertainty of 10 % at 300 K, $\bar{v}$ is the root-mean-square velocity of GSA molecules, S is the aerosol surface concentration (μm^2 cm^{-3}), and γ is the uptake coefficient of GSA on aerosol surface. A value of 0.73 ± 0.21 (Jefferson et al., 1997) is adopted for γ. Because OH is not measured in this work, the OH concentration is estimated according to Ehhalt and Rohrer (2000),

$$[\mathrm{OH}] = a(J_{\mathrm{O^1D}})^{\alpha}(J_{\mathrm{NO_2}})^{\beta}\frac{b\mathrm{NO_2}+1}{c\mathrm{NO_2^2}+d\mathrm{NO_2}+1} \tag{3}$$

where $J_{\mathrm{O^1D}}$ and $J_{\mathrm{NO_2}}$ are observed photolysis rates of O_3 and NO_2, respectively. The values of the constants are taken from Ehhalt and Rohrer (2000), i.e. $a = 4.1 \times 10^9$, $b = 140$, $c = 0.41$, $d = 1.7$, $\alpha = 0.83$, and $\beta = 0.19$. It has been suggested that Eq. (3) is valid under high NO_x conditions, which is typically the case in the megacity Beijing with large NO_x emissions (Liu and Shao, 2007). The major uncertainty in the OH calculation originates from the coefficients used in Eq. (3). To validate the OH calculation, we use Eq. (3) to estimate the OH concentration at the Yufa site during the CAREBeijing 2006 field campaign and compare the results with the in-situ measurements. The OH measurement at Yufa was conducted with a laser induced fluorescence (LIF) system developed at Forschungszentrum Jülich, Germany. A detailed description of the OH measurement has been provided by Lu et al. (2011). Briefly, ambient air was sampled through a 0.4 mm orifice into a low-pressure chamber, where OH was excited at 308 nm and detected by the resulting resonance fluorescence between 307 nm and 311 nm. The LIF instrument was calibrated with an OH source based on the photolysis of water vapor by 184.9 nm radiation from a mercury lamp. For 5-min average time, the detection limit was about 5×10^5 molecules cm^{-3}. The accuracy of the OH calibration method was about 10 %. During the measurement period, day to day calibration showed a variability of 9 % (Lu et al., 2011). Hence, we estimate an uncertainty of about 19 % in the OH measurement at Yufa. A linear regression between the calculated and the measured OH concentrations at daytime (i.e. $J_{\mathrm{O^1D}}$ and $J_{\mathrm{NO_2}} > 0$) shows a slope of 0.71, an intercept of -0.4×10^6 molecules cm^{-3} and a R^2 of 0.65. The negative intercept is within the instrument detection limit. The correlation and regression results indicate the validity of using above coefficients for Beijing. Given that the Yufa site is located near a highway and influenced by traffic emissions, which is the same as PKU site, we therefore estimate the uncertainty of the OH calculation is within 48 %.

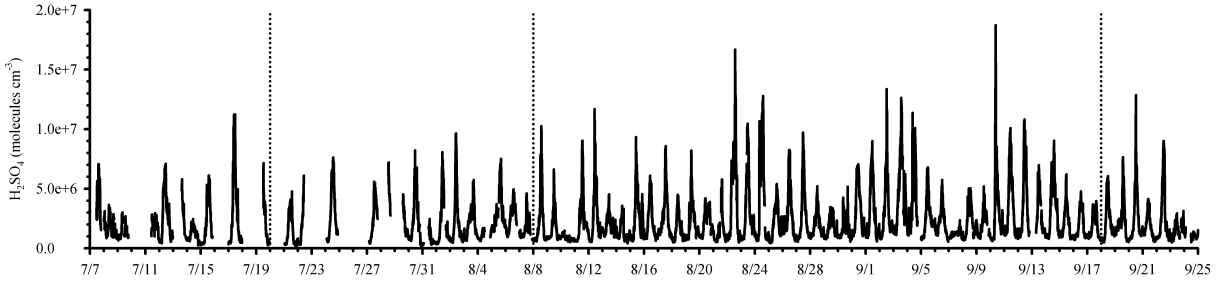

Fig. 3. Time series of 10 min averaged GSA concentration observed from 7 July to 25 September during the CAREBeijing 2008 Campaign. The dotted lines indicate the date of implementation of some major emission control measures, i.e. 20 July when odd/even plate number rule was applied, 8 August when full-scale control was applied, and 18 September when the regulations were loosened.

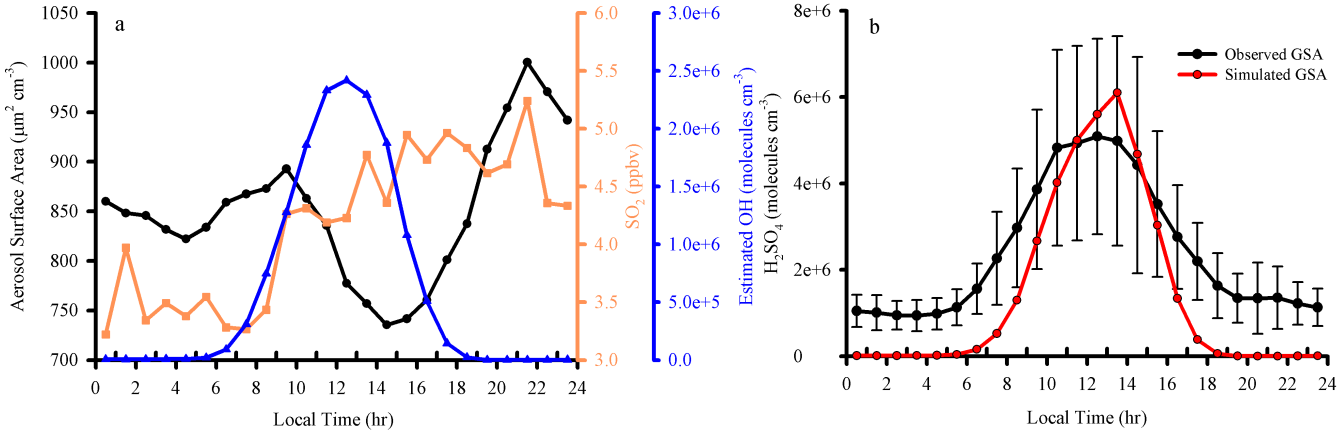

Fig. 4. (a) Hourly average diurnal profiles of aerosol surface area, SO_2, and modeled OH from 7 July to 25 September; **(b)** calculated (red) and measured (black) diurnal profiles of GSA.

Similarly, the uncertainties associated with the GSA simulation arise from the parameters used in Eq. (2), including the measured SO_2 concentration, the calculated OH concentration, the termolecular rate constant of Reaction (R1), the GSA uptake coefficient, and the measured aerosol surface area. Specifically, SO_2 is measured with a relatively small uncertainty of 1 %. The OH is calculated with an uncertainty of 48 %. The aerosol surface area measurement contains an uncertainty of 10 %. The rate constant of Reaction (R1) is taken from JPL (2006) with an uncertainty of 10 % at 300 K. The GSA uptake coefficient is taken from Jefferson et al. (1997) with an uncertainty of 29 %. Therefore, the overall uncertainty of the simulated GSA concentration can be about 98 %.

Because only dry deposition is considered in Eq. (2), GSA measurements when precipitation occurs are excluded in this investigation. Figure 4a shows hourly average diurnal plots of the measured aerosol surface area, SO_2, and calculated OH concentration. Figure 4b displays both the hourly average GSA measurements with one standard deviation (σ) error bar and calculated GSA from Eq. (2). Daytime GSA reaches a daily maximum around noontime with a value of $\sim 5 \times 10^6$ molecules cm^{-3}. The calculated GSA captures the measured trend in general, indicating that photochemistry dominates the GSA production. However, since photochemistry is the only source considered, nighttime GSA cannot be accounted for. Given that the lifetime of GSA relative to aerosol uptake is less than a minute, the nighttime concentration of GSA ($\sim 1 \times 10^6$ molecules cm^{-3}) clearly indicates that other non-photochemical mechanism is operative to produce OH radicals, such as the ozonolysis of alkenes (Zhang et al., 2002a; Fan and Zhang, 2004). The planetary boundary layer height typically reaches the minimum in the early morning and grows rapidly within a few hours after sunrise. As a result, surface air pollutants are vented upward and air masses of the regional sources are mixed down, explaining the variations in the particle surface area concentration and SO_2 concentration. Both OH and GSA are photochemically driven and their concentrations show clear variations with the solar diurnal cycle.

Another interesting feature in Fig. 3 is that the measured GSA peak value exhibits a periodic variation of about one week. Such a variation is related to the aerosol loading, which is regulated by the large-scale weather pattern in this

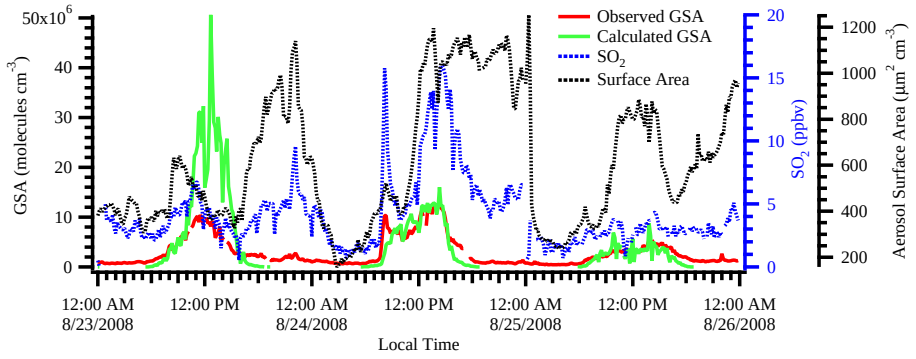

Fig. 5. Time series of both observed (red trace) and calculated (green trace) GSA from 23 to 25 August. Also shown here are the SO_2 (blue dot) and aerosol surface area (black dot) used in GSA simulations.

area. A change in the weather pattern, such as the wind direction (from northwest) or precipitation, leads to a cleaner air condition, allowing GSA to reach a higher concentration. At the PKU site, the barometric pressure was also found varying sinusoidally with a period of 5 to 10 days. Most of the high GSA episodes were detected during the transitions periods. In addition, higher GSA concentration periods were often associated with northerly wind. T. Wang et al. (2010) suggested that a weak high-pressure system over the Hebei province (to the south of Beijing) led to the two pollution episodes on 23–29 July and 4–9 August, when high PM_{10} mass loading (T. Wang et al., 2010) but low GSA concentration were observed.

To further clarify the GSA formation and the ensuing gas/particle conversion process, time series of both observed and calculated GSA from 23–25 August are displayed in Fig. 5. Also shown in Fig. 5 are the SO_2 and aerosol surface area used in Eq. (2). 23 August is a nucleation day, characterized by low pre-existing aerosol loading. Since the nucleation term is not considered in Eq. (2), the calculated GSA is substantially higher than the observation after 09:30, when nucleation starts. The simulated high GSA concentration is also a result of low surface area, especially when SO_2 is also relatively low. On both 24 and 25 August, the calculation matches the observation very well, indicating that GSA is mainly governed by Eq. (2) despite the significant variations in both SO_2 and aerosol surface area.

In order to improve air quality during the Olympic Games, control measures have been implemented to reduce primary air pollutant emissions, especially from industries, on-road vehicles and construction sites. Considerable reductions in both gas-phase and aerosol-phase pollutants have been observed by both mobile laboratory (Wang et al., 2009) and surface stations (T. Wang et al., 2010). Moreover, more precipitation and cleaner conditions associated with the northerly wind were experienced during the period. Consequently, more "Blue-Sky" days were observed during the Olympic Games in the Beijing region (Zhang et al., 2010). Compared to the period prior to 8 August, at the PKU site daytime (06:00 a.m. to 06:00 p.m.) average SO_2 increased from 3.7 to 4.5 ppbv while aerosol surface area decreased from 1.0×10^3 to 0.57×10^3 $\mu m^2\,cm^{-3}$ during the Olympic Games period (8–24 August). Meanwhile, the calculated OH concentration increased from 0.4×10^6 to 1.9×10^6 molecules cm^{-3}. The unexpected increase in SO_2 was probably due to the fact that SO_2 in Beijing was controlled by regional sources. Since GSA production can be enhanced by stronger actinic flux and uptake by preexisting aerosol surfaces represents the dominant sink for GSA, an increasing trend in the daily GSA concentration is evident in Fig. 3, especially during the Olympics and Paralympics period, when more stringent air quality control measures were adopted. Consequently, the frequency of the peak H_2SO_4 concentration exceeding 5×10^6 molecule cm^{-3} increases by 16 % during 8–24 August, compared to the time period prior to 8 August. This trend is consistent with that of the frequency of new particle formation events (Yue et al., 2010).

3.3 H_2SO_4 in new particle formation

During the CAREBeijing 2008 campaign, fourteen nucleation events were observed, which have been discussed previously in a companion paper in this special issue (Yue et al., 2010). The criterion for discerning these so-called new particle formation events was the burst in the nucleation mode particle concentration (Birmili and Wiedensohler, 2000). In this study, particles between 3 and 10 nm were considered to represent the newly formed particles. One burst was counted as new particle formation event if the duration time was longer than 2.5 h and the maximum number concentration of 3–10 nm particles was larger than 10^4 cm^{-3}. The events with bursts in the 3- to 10-nm size range, lasting a short time but without the growth of 3- to 10-nm particles to larger sizes, were not included in new particle formation events discussed in this study. In the calculation of nucleation rate, the particle number size distributions at ambient RH were used. The particle number size distributions at ambient RH were calculated based on the measured dry number size distributions and

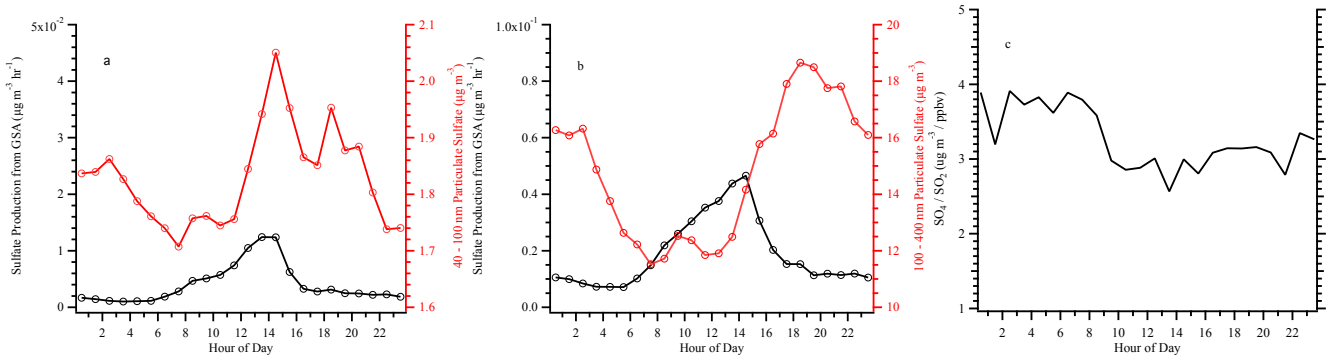

Fig. 6. (a) Diurnal profiles of condensation rates of GSA onto Aitken mode aerosols (40–100 nm) and sulfate concentrations in Aitken mode; **(b)** diurnal profiles of condensation rates of GSA onto accumulation mode particles (100–400 nm) and sulfate concentrations in accumulation mode; **(c)** diurnal profile of PM_1 sulfate (SO_4) to SO_2 ratio.

the calculated size-dependent hygroscopic growth factors at ambient RH. Hygroscopic growth factors of the nucleation mode particles are obtained from Biskos et al. (2009), and those of larger particles are calculated from our earlier size-dependent measurements at 90 % RH (Laakso et al., 2004). In this work, a multivariate statistical method (MSM) (McGraw and Zhang, 2008) is employed to analyze the molecular components of the critical nuclei during ten nucleation events. Table 1 summarizes new particle formation rate (FR) and GSA measurements.

To perform the MSM analysis, a multicomponent extension form of the kinetic nucleation theorem (Ford, 1997) is deduced by treating the critical clusters as the transition state during the nucleation process, i.e. the nucleation rate is determined from the sum of flux of each condensable gas that contributes to the growth of clusters over the critical size. Details of the MSM analysis for aerosol nucleation are described by McGraw and Zhang (2008). Applying the data listed in Table 1, we find that the most likely number of H_2SO_4 molecules in the critical clusters is 2. This is consistent with the result by Anderson et al. (2008), who suggest that at least two sulfuric acid molecules are required to form a stable critical cluster. It should be pointed out that other species, including organics, can also be present in the critical nucleus (Zhang et al., 2004, 2009; Metzger et al., 2010), but cannot be concluded from our present analysis.

3.4 Contribution of GSA to particulate sulfate

To evaluate the likely contribution of GSA to particulate sulfate, we compare the calculated condensation rates to the measured sulfate mass concentrations by the HR-ToF-AMS. Figure 6a and b show the diurnal profiles of the calculated GSA condensation rates for the Aitken and accumulation modes, which are evaluated using Eq. (2). The aerosol surface area of each mode is integrated from TDMPS number size distribution measurement. Also shown in Fig. 6a and b for comparison are diurnal profiles of the corresponding

Table 1. Summary of nucleation events during the CAREBeijing 2008 field study including aerosol formation rate (FR), GSA concentration, and relative humidity (RH %) that used in the multivariate analysis to evaluate the number of sulfuric acid molecule in the critical cluster.

Date	FR ($cm^{-3}\,s^{-1}$)	H_2SO_4 ($10^6\,cm^{-3}$)	RH %
12-Jul	7.3	5.0	27.8
17-Jul	13.2	7.1	40.8
1-Aug	6.9	4.8	58.9
12-Aug	13.2	7.4	63.4
15-Aug	8.7	5.5	51.5
18-Aug	2.1	3.2	50.5
23-Aug	7.3	6.3	41.2
31-Aug	5.8	4.5	47.3
1-Sep	4.2	5.3	40.8
18-Sep	2.4	4.0	44.3

aerosol sulfate mass concentrations for the Aitken and accumulation modes measured by the HR-ToF-AMS. Limited by the sampling efficiency of the HR-ToF-AMS, we define Aitken and accumulation modes as 40 to 100 nm and 100 to 400 nm in Stokes diameters, respectively. Both modes of aerosol sulfate show signature of predominant secondary formation, i.e. the lowest concentration in the early morning and the highest concentration in either the afternoon or early evening. The calculated GSA condensation rate in both modes is strongly influenced by the GSA concentration (Fig. 4b). For the Aitken mode aerosols, the calculated GSA condensation rate exhibits a correlation with the measured concentration of sulfate mass from the HR-ToF-AMS. This may imply that condensation of GSA (followed by neutralization with ammonia) dominates particle growth in the mode. In contrast, for the case of accumulation mode aerosols, the increase in the concentration of sulfate

mass from the HR-ToF-AMS is noticeably delayed relative to that of the calculated GSA condensation rate, suggesting that GSA condensation hardly contributes to the growth in this mode. The high sulfate concentration measured at the PKU site might be a result of accumulated oxidation process, occurring over many days since the time of emission. Moreover, the GSA productions are likely much higher in the source regions, which are primarily industrial areas with much more concentrated SO_2. As shown in Fig. 6c, the PM_1 sulfate to SO_2 ratio has little diurnal variation, indicating that most aerosol sulfate has been formed before arriving at the PKU site. Therefore, it is reasonable to use the hour-average of the whole data set to investigate the correlation between the diurnal variations of sulfate and GSA. From this work, we obtain an average of $0.6\,\mu g\,m^{-3}$ per day sulfate production from the GSA condensation. Given that $PM_{1.0}$ sulfate has a daily average concentration of $\sim 17\,\mu g\,m^{-3}$ and a residence time of 3 to 7 days, GSA condensation can contribute to 10–25 % of PM_1 sulfate. Furthermore, the slight decreasing trend in Fig. 6c indicates that air mass with less sulfate but more SO_2 is mixed down, which makes sulfate productions through cloud processing less likely.

It has been suggested by Guo et al. (2010) that fine mode sulfate in the Beijing area can mainly arise from secondary sources, since no indications of primary contributions from either biomass burning or automobile exhausts were found. Also, according to He et al. (2010), sulfate production through the aqueous phase reaction between hydrogen peroxides (H_2O_2) and SO_2

$$SO_2 + H_2O \leftrightarrow HSO_3^- + H^+ \quad \text{(R4)}$$

$$HSO_3^- + H_2O_2 \rightarrow HSO_4^- + H_2O \quad \text{(R5)}$$

in aqueous aerosols is not significant during the CAREBeijing 2008 campaign. Other possible sulfate production mechanisms include heterogeneous reactions on the aerosol surface or in-cloud processing (Seinfeld and Pandis, 1998). Future work, especially a detailed aerosol dynamic model along with other aerosol and gaseous measurements, is required to quantitatively assess the contributions of GSA condensation, inter-modal coagulation, and other sulfate production mechanisms to the measured sulfate mass concentrations in the Aitken and accumulation modes.

4 Conclusions

As part of the CAREBeijing 2008 field study, GSA measurement by AP-ID-CIMS was conducted at an urban site in Beijing City from 7 July 2008 to 25 September 2008. This represents the first GSA measurements in China. Data quality is examined using a normalized sequential difference procedure. GSA data set shows no statistically significant systematic errors. Correlations between GSA and meteorology parameters are also analyzed. Only a minor bias is identified when the wind direction is perpendicular to the sample inlet, likely due to turbulence-induced wall losses. Diurnally, GSA shows strong dependence on actinic flux and reaches daily maximum around noon, ranging from a few 10^6 to 1.9×10^7 molecules cm^{-3}. Nighttime GSA ($\sim 1 \times 10^6$ molecules cm^{-3}) is also observed, indicating that non-photochemical OH sources are operative in Beijing, such as the ozonolysis of alkenes. Traffic control and other administrative measures pertaining to the Olympic Games period appear to be effectively improving air quality in Beijing with significant reduction in aerosol loading, which is consistent with the observation that GSA daily maximum is noticeably increased from the beginning to the later part of the campaign. On the basis of the assumption that GSA concentration is governed by photochemical production and aerosol surface condensation loss, a steady state calculation is performed to evaluate GSA chemistry in Beijing. In general, simulated GSA captures the diurnal variations of measured GSA, indicating that condensation on preexisting aerosol surface corresponds to the dominant loss mechanism of GSA. Hence, GSA can potentially contribute to the aerosol aging process, considerably altering aerosol optical properties and hygroscopicity. GSA time series show a wave shape pattern characterized by accumulation of aerosol followed by a washout. Analysis of the critical cluster composition using a multivariate statistical method indicates the presence of two sulfuric acid molecules. The calculated condensation rate of H_2SO_4 correlates with the daytime sulfate mass concentration of the Aitken mode, but not that of the accumulation mode aerosols. The results imply that condensation of GSA at the concentrations measured in Beijing can only contribute to 10–25 % of PM_1 sulfate formation, indicating that either much stronger sulfate production exists at the SO_2 source region or other sulfate production mechanisms are responsible for the sulfate production.

Acknowledgements. This work was part of the Campaign of Atmospheric Research in Beijing and surrounding areas supported by Beijing Environment Protection Bureau (OITC-G08026056) and the National Natural Science Foundation of China (20977001, 21025728). This work was also supported by the Robert A. Welch Foundation (Grant A-1417). R. Z. acknowledged further support from the National Natural Science Foundation of China Grant (40728006).

Edited by: D. Parrish

References

Anderson, K. E., Siepmann, J. I., McMurry, P. H., and VandeVondele, J.: Importance of the number of acid molecules and the strength of the base for double-ion formation in $(H_2SO_4)_m \cdot Base \cdot (H_2O)_6$Clusters, J. Am. Chem. Soc., 130, 14144–14147, doi:10.1021/ja8019774, 2008.

Arnold, F.: Atmospheric aerosol and cloud condensation nuclei formation: A possible influence of cosmic rays?, Space Sci. Rev., 125, 169–186, 2006.

Arnold, J. R., Hartsell, B. E., Luke, W. T., Ullah, S. M. R., Dasgupta, P. K., Huey, L. G., and Tate, P.: Field test of four methods for gas-phase ambient nitric acid, Atmos. Environ., 41, 4210–4226, doi:10.1016/j.atmosenv.2006.07.058, 2007.

Birmili, W. and Wiedensohler, A.: New particle formation in the continental boundary layer: Meteorological and gas phase parameter influence, Geophys. Res. Lett., 27, 3325–3328, 2000.

Biskos, G., Buseck, P. R., and Martin, S. T.: Hygroscopic growth of nucleation-mode acidic sulfate particles, J. Aerosol Sci., 40, 338–347, doi:10.1016/j.jaerosci.2008.12.003, 2009.

Bohn, B., Corlett, G. K., Gillmann, M., Sanghavi, S., Stange, G., Tensing, E., Vrekoussis, M., Bloss, W. J., Clapp, L. J., Kortner, M., Dorn, H.-P., Monks, P. S., Platt, U., Plass-Dülmer, C., Mihalopoulos, N., Heard, D. E., Clemitshaw, K. C., Meixner, F. X., Prevot, A. S. H., and Schmitt, R.: Photolysis frequency measurement techniques: results of a comparison within the ACCENT project, Atmos. Chem. Phys., 8, 5373–5391, doi:10.5194/acp-8-5373-2008, 2008.

Chan, C. K. and Yao, X.: Air pollution in mega cities in China, Atmos. Environ., 42, 1–42, doi:10.1016/j.atmosenv.2007.09.003, 2008.

Cheng, Y. F., Wiedensohler, A., Eichler, H., Su, H., Gnauk, T., Brueggemann, E., Herrmann, H., Heintzenberg, J., Slanina, J., Tuch, T., Hu, M., and Zhang, Y. H.: Aerosol optical properties and related chemical apportionment at Xinken in Pearl River Delta of China, Atmos. Environ., 42, 6351–6372, doi:10.1016/j.atmosenv.2008.02.034, 2008.

Cheng, Y. F., Berghof, M., Garland, R. M., Wiedensohler, A., Wehner, B., Muller, T., Su, H., Zhang, Y. H., Achtert, P., Nowak, A., Poschl, U., Zhu, T., Hu, M., and Zeng, L. M.: Influence of soot mixing state on aerosol light absorption and single scattering albedo during air mass aging at a polluted regional site in northeastern China, J. Geophys. Res., 114, D00G10, doi:10.1029/2008jd010883, 2009.

DeCarlo, P. F., Kimmel, J. R., Trimborn, A., Northway, M. J., Jayne, J. T., Aiken, A. C., Gonin, M., Fuhrer, K., Horvath, T., Docherty, K. S., Worsnop, D. R., and Jimenez, J. L.: Field-deployable, high-resolution, time-of-flight aerosol mass spectrometer, Anal. Chem., 78, 8281–8289, 2006.

Ehhalt, D. H. and Rohrer, F.: Dependence of the OH concentration on solar UV, J. Geophys. Res., 105, 3565–3571, 2000.

Fan, J. W. and Zhang, R. Y.: Atmospheric Oxidation Mechanism of Isoprene, Environ. Chem., 1, 140–149, doi:10.1071/en04045, 2004.

Finlayson-Pitts, B. J. and Pitts, J. N.: Chemistry of the upper and lower atmosphere : theory, experiments and applications, Academic Press, San Diego, Calif., 969 pp., 1999.

Ford, I. J.: Nucleation theorems, the statistical mechanics of molecular clusters, and a revision of classical nucleation theory, Phys. Rev. E, 56, 5615–5629, 1997.

Fortner, E. C., Zhao, J., and Zhang, R. Y.: Development of ion drift-chemical ionization mass spectrometry, Anal. Chem., 76, 5436–5440, doi:10.1021/Ac0493222, 2004.

Freiberg, J. E. and Schwartz, S. E.: Oxidation of SO_2 in aqueous droplets – mass-transport limitation in laboratory studies and the ambient atmosphere, Atmos. Environ., 15, 1145–1154, 1981.

Guo, S., Hu, M., Wang, Z. B., Slanina, J., and Zhao, Y. L.: Size-resolved aerosol water-soluble ionic compositions in the summer of Beijing: implication of regional secondary formation, Atmos. Chem. Phys., 10, 947–959, doi:10.5194/acp-10-947-2010, 2010.

He, S. Z., Chen, Z. M., Zhang, X., Zhao, Y., Huang, D. M., Zhao, J. N., Zhu, T., Hu, M., and Zeng, L. M.: Measurement of atmospheric hydrogen peroxide and organic peroxides in Beijing before and during the 2008 Olympic Games: chemical and physical factors influencing their concentrations, J. Geophys. Res., 115, D17307, doi:10.1029/2009JD013544, 2010.

Huang, X.-F., He, L.-Y., Hu, M., Canagaratna, M. R., Sun, Y., Zhang, Q., Zhu, T., Xue, L., Zeng, L.-W., Liu, X.-G., Zhang, Y.-H., Jayne, J. T., Ng, N. L., and Worsnop, D. R.: Highly time-resolved chemical characterization of atmospheric submicron particles during 2008 Beijing Olympic Games using an Aerodyne High-Resolution Aerosol Mass Spectrometer, Atmos. Chem. Phys., 10, 8933–8945, doi:10.5194/acp-10-8933-2010, 2010.

IPCC: IPCC Fourth Assessment Report: Climate change 2007: the physical science basis, edited by: Solomon, S., Qin, D., Manning, M., Chen, Z., Marquis, M., Averyt, K. B., Tignor, M., and Miller, H. L., Cambridge Univ. Press, United Kingdom and New York, 996 pp., 2007.

Jefferson, A., Eisele, F. L., Ziemann, P. J., Weber, R. J., Marti, J. J., and McMurry, P. H.: Measurements of the H_2SO_4 mass accommodation coefficient onto polydisperse aerosol, J. Geophys. Res., 102, 19021–19028, 1997.

JPL: Chemical kinetics and photochemical data for use in atmospheric studies Evaluation 15, NASA, JPL, Caltech, Pasadena, Calif., 523 pp., 2006.

Khalizov, A. F., Xue, H. X., Wang, L., Zheng, J., and Zhang, R. Y.: Enhanced light absorption and scattering by carbon soot aerosol internally mixed with sulfuric acid, J. Phys. Chem. A, 113, 1066–1074, doi:10.1021/jp807531n, 2009a.

Khalizov, A. F., Zhang, R. Y., Zhang, D., Xue, H. X., Pagels, J., and McMurry, P. H.: Formation of highly hygroscopic soot aerosols upon internal mixing with sulfuric acid vapor, J. Geophys. Res., 114, D05208, doi:10.1029/2008jd010595, 2009b.

Kulmala, M., Vehkamaki, H., Petaja, T., Dal Maso, M., Lauri, A., Kerminen, V. M., Birmili, W., and McMurry, P. H.: Formation and growth rates of ultrafine atmospheric particles: a review of observations, J. Aerosol Sci., 35, 143–176, 2004.

Laakso, L., Petäjä, T., Lehtinen, K. E. J., Kulmala, M., Paatero, J., Hõrrak, U., Tammet, H., and Joutsensaari, J.: Ion production rate in a boreal forest based on ion, particle and radiation measurements, Atmos. Chem. Phys., 4, 1933–1943, doi:10.5194/acp-4-1933-2004, 2004.

Liu, Y. and Shao, M.: Estimation and prediction of black carbon emissions in Beijing City, Chin. Sci. Bull., 52, 1274–1281, doi:10.1007/s11434-007-0162-8, 2007.

Lu, K. D., Rohrer, F., Holland, F., Fuchs, H., Bohn, B., Brauers, T., Chang, C. C., Häseler, R., Hu, M., Kita, K., Kondo, Y., Li, X., Lou, S. R., Nehr, S., Shao, M., Zeng, L. M., Wahner, A., Zhang, Y. H., and Hofzumahaus, A.: Observation and modelling of OH and HO_2 concentrations in the Pearl River Delta 2006: a missing OH source in a VOC rich atmosphere, Atmos. Chem. Phys. Discuss., 11, 11311–11378, doi:10.5194/acpd-11-11311-2011, 2011.

McGraw, R. and Zhang, R. Y.: Multivariate analysis of homoge-

neous nucleation rate measurements. Nucleation in the p-toluic acid/sulfuric acid/water system, J. Chem. Phys., 128, 064508, doi:10.1063/1.2830030, 2008.

Metzger, A., Verheggen, B., Dommen, J., Duplissy, J., Prevot, A. S. H., Weingartner, E., Riipinen, I., Kulmala, M., Spracklen, D. V., Carslaw, K. S., and Baltensperger, U.: Evidence for the role of organics in aerosol particle formation under atmospheric conditions, P. Natl. Acad. Sci. USA, 107, 6646–6651, doi:10.1073/pnas.0911330107, 2010.

Molina, M. J., Molina, L. T., Zhang, R. Y., Meads, R. F., and Spencer, D. D.: The reaction of $ClONO_2$ with HCl on aluminum oxide, Geophys. Res. Letts., 24, 1619–1622, 1997.

Nadykto, A. B. and Yu, F. Q.: Strong hydrogen bonding between atmospheric nucleation precursors and common organics, Chem. Phys. Lett., 435, 14–18, doi:10.1016/j.cplett.2006.12.050, 2007.

Seeley, J. V., Jayne, J. T., and Molina, M. J.: High-pressure fast-flow technique for gas-phase kinetics studies, Int. J. Chem. Kinet., 25, 571–594, 1993.

Seinfeld, J. H. and Pandis, S. N.: Atmospheric chemistry and physics: from air pollution to climate change, Wiley, New York, 1326 pp., 1998.

Sipila, M., Berndt, T., Petaja, T., Brus, D., Vanhanen, J., Stratmann, F., Patokoski, J., Mauldin, R. L., Hyvarinen, A. P., Lihavainen, H., and Kulmala, M.: The role of sulfuric acid in atmospheric nucleation, Science, 327, 1243–1246, doi:10.1126/science.1180315, 2010.

Suh, I., Lei, W. F., and Zhang, R. Y.: Experimental and theoretical studies of isoprene reaction with NO_3, J. Phys. Chem. A, 105, 6471–6478, 2001.

Wang, L., Khalizov, A. F., Zheng, J., Xu, W., Ma, Y., Lal, V., and Zhang, R.: Atmospheric nanoparticles formed from heterogeneous reactions of organics, Nat. Geosci., 3, 238–242, doi:10.1038/ngeo778, 2010.

Wang, M., Zhu, T., Zheng, J., Zhang, R. Y., Zhang, S. Q., Xie, X. X., Han, Y. Q., and Li, Y.: Use of a mobile laboratory to evaluate changes in on-road air pollutants during the Beijing 2008 Summer Olympics, Atmos. Chem. Phys., 9, 8247–8263, doi:10.5194/acp-9-8247-2009, 2009.

Wang, T., Nie, W., Gao, J., Xue, L. K., Gao, X. M., Wang, X. F., Qiu, J., Poon, C. N., Meinardi, S., Blake, D., Wang, S. L., Ding, A. J., Chai, F. H., Zhang, Q. Z., and Wang, W. X.: Air quality during the 2008 Beijing Olympics: secondary pollutants and regional impact, Atmos. Chem. Phys., 10, 7603–7615, doi:10.5194/acp-10-7603-2010, 2010.

Yue, D. L., Hu, M., Zhang, R. Y., Wang, Z. B., Zheng, J., Wu, Z. J., Wiedensohler, A., He, L. Y., Huang, X. F., and Zhu, T.: The roles of sulfuric acid in new particle formation and growth in the mega-city of Beijing, Atmos. Chem. Phys., 10, 4953–4960, doi:10.5194/acp-10-4953-2010, 2010.

Young, L. H., Benson, D. R., Kameel, F. R., Pierce, J. R., Junninen, H., Kulmala, M., and Lee, S.-H.: Laboratory studies of H2SO4/H2O binary homogeneous nucleation from the SO_2+OH reaction: evaluation of the experimental setup and preliminary results, Atmos. Chem. Phys., 8, 4997–5016, doi:10.5194/acp-8-4997-2008, 2008.

Zhang, D. and Zhang, R. Y.: Laboratory investigation of heterogeneous interaction of sulfuric acid with soot, Environ. Sci. Technol., 39, 5722–5728, 2005.

Zhang, D., Lei, W. F., and Zhang, R. Y.: Mechanism of OH formation from ozonolysis of isoprene: kinetics and product yields, Chem. Phys. Lett., 358, 171–179, 2002a.

Zhang, D., Zhang, R. Y., Park, J., and North, S. W.: Hydroxy peroxy nitrites and nitrates from OH initiated reactions of isoprene, J. Am. Chem. Soc., 124, 9600–9605, doi:10.1021/ja0255195, 2002b.

Zhang, Q. H., Zhang, J. P., and Xue, H. W.: The challenge of improving visibility in Beijing, Atmos. Chem. Phys., 10, 7821–7827, doi:10.5194/acp-10-7821-2010, 2010.

Zhang, R. Y.: Getting to the critical nucleus of aerosol formation, Science, 328, 1366–1367, doi:10.1126/science.1189732, 2010.

Zhang, R. Y., Wooldridge, P. J., Abbatt, J. P. D., and Molina, M. J.: Physical-chemistry of the H_2SO_4/H_2O binary-system at low-temperatures – stratospheric implications, J. Phys. Chem., 97, 7351–7358, 1993a.

Zhang, R. Y., Wooldridge, P. J., and Molina, M. J.: Vapor-pressure measurements for the $H_2SO_4/HNO_3/H_2O$ and $H_2SO_4/HCl/H_2O$ systems - incorporation of stratospheric acids into background sulfate aerosols, J. Phys. Chem., 97, 8541–8548, 1993b.

Zhang, R. Y., Leu, M. T., and Molina, M. J.: Formation of polar stratospheric clouds on preactivated background aerosols, Geophys. Res. Letts., 23, 1669–1672, doi:10.1029/96gl01133, 1996.

Zhang, R. Y., Suh, I., Zhao, J., Zhang, D., Fortner, E. C., Tie, X. X., Molina, L. T., and Molina, M. J.: Atmospheric new particle formation enhanced by organic acids, Science, 304, 1487–1490, 2004.

Zhang, R. Y., Li, G. H., Fan, J. W., Wu, D. L., and Molina, M. J.: Intensification of Pacific storm track linked to Asian pollution, P. Natl. Acad. Sci. USA, 104, 5295–5299, doi:10.1073/pnas.0700618104, 2007.

Zhang, R. Y., Khalizov, A. F., Pagels, J., Zhang, D., Xue, H. X., and McMurry, P. H.: Variability in morphology, hygroscopicity, and optical properties of soot aerosols during atmospheric processing, P. Natl. Acad. Sci. USA, 105, 10291–10296, doi:10.1073/pnas.0804860105, 2008.

Zhang, R. Y., Wang, L., Khalizov, A. F., Zhao, J., Zheng, J., McGraw, R. L., and Molina, L. T.: Formation of nanoparticles of blue haze enhanced by anthropogenic pollution, P. Natl. Acad. Sci. USA, 106, 17650–17654, doi:10.1073/pnas.0910125106, 2009.

Zhao, J., Levitt, N. P., and Zhang, R. Y.: Heterogeneous chemistry of octanal and 2,4-hexadienal with sulfuric acid, Geophys. Res. Lett., 32, L09802, doi:10.1029/2004gl022200, 2005.

Zhao, J., Levitt, N. P., Zhang, R. Y., and Chen, J. M.: Heterogeneous reactions of methylglyoxal in acidic media: Implications for secondary organic aerosol formation, Environ. Sci. Technol., 40, 7682–7687, doi:10.1021/es060610k, 2006.

Zhao, J., Khalizov, A., Zhang, R. Y., and McGraw, R.: Hydrogen-bonding interaction in molecular complexes and clusters of aerosol nucleation precursors, J. Phys. Chem. A, 113, 680–689, doi:10.1021/jp806693r, 2009.

Zheng, J., Khalizov, A., Wang, L., and Zhang, R.: Atmospheric pressure-ion drift chemical ionization mass spectrometry for detection of trace gas species, Anal. Chem., 82, 7302–7308, doi:10.1021/ac101253n, 2010.